High temperature corrosion behaviour of calcium magnesium aluminosilicate coated oxide-oxide ceramic matrix composites

Ramachandran, K., Bear, J. C. & Jayaseelan, D. D.

DOI 10.1016/j.ceramint.2023.10.214
ISSN 0272-8842
ESSN 1873-3956

Publisher: Elsevier

Ceramics International xxx (xxxx) xxx

Contents lists available at ScienceDirect

Ceramics International

journal homepage: www.elsevier.com/locate/ceramint

High temperature corrosion behaviour of calcium magnesium aluminosilicate coated oxide-oxide ceramic matrix composites

Karthikeyan Ramachandran [a,b,*], Joseph C. Bear [c], Doni Daniel Jayaseelan [a,**]

[a] Department of Aerospace and Aircraft Engineering, Kingston University, Roehampton Vale Campus, London, SW15 3DW, United Kingdom
[b] School of Mechanical Engineering, Coventry University, Coventry, CV1 2JH, United Kingdom
[c] Department of Chemical and Pharmaceutical Sciences, Kingston University, Penrhyn Road, Kingston upon Thames, KT1 2EE, United Kingdom

ARTICLE INFO

Handling Editor: Dr P. Vincenzini

Keywords:
Oxide-oxide CMCs
CMAS
Dip coatings
Corrosion behaviour
Fracture Toughness

ABSTRACT

Corrosion on turbine blades in calcium magnesium alumino-silicate (CMAS) environment is a crucial failure for turbine engines and its components. In this study, oxide-oxide (O-O) ceramic matrix composites (CMCs) (AS-N610), the potential materials for gas turbine components are examined for its corrosion behaviour at high temperatures at various intervals of time in presence of CMAS. The corrosion studies indicated that dip coated with CMAS revealed a weight gain of ~3% owing to the formation of α-Al_2O_3 at 1400 °C. The SE images indicated cracks at the interface due to thermal mismatch between CMAS and O-O substrate. With increase in corrosion time, cracks at the interface propagated onto the matrix and fibres of O-O CMCs. This crack propagation is attributed to the diffusion of calcium aluminosilicate (CAS) with small traces of Mg which wicks the columns of O-O CMCs. Indentation fracture toughness of O-O CMCs degraded by ~22% for 1400 °C in presence of CMAS compared to un-corroded sample.

1. Introduction

Ceramics matrix composites (CMCs) are promising candidates towards hot sections components of gas turbines as an alternative to superalloys owing to their weight to thrust ratio, chemical stability and excellent materials properties at high temperatures [1,2]. Various countries including USA, Europe and Japan have been considering CMCs for rotating and static components with projects like Integrated High Performance Turbine Engine Technology (IHPTET) [3]. Even with their promising thermo-mechanical properties, CMCs are vulnerable to corrosion in water vapour and CMAS environments at high temperature like SiC/SiC CMCs undergoing recession in water vapour environment owing to formation of $Si(OH)_4$ [4,5]. Thus, protective coatings such as thermal/environmental barrier coatings (T/EBCs) are utilised to protect the gas-turbine (GT) engine for hot section components like aircraft propulsion, power generation and marine propulsion to protect CMCs from corrosion [6,7]. Hence, it is necessary to have good corrosion resistance towards molten calcium-magnesium aluminosilicate (CMAS) and water vapour towards hot-section components [8,9].

CMAS corrosion attack occurs when atmospheric dust such as sand, volcanic ash and other silica particles gets deposited on to the surfaces of coatings/turbine blade which further melts and enter porous gaps leading to wicking of the column resulting in cracks and spallation [10,11]. Various research on understanding the effects of CMAS corrosion on turbine materials and thermal/environmental barrier coatings (T/EBCs) and its mitigation have been attempted in past few decades [6,12,13,14]. Approaches like de-wetting of outer layer has been utilised to mitigate the corrosion, however during thermal cycling operations these outer layers cracked or eroded [15]. Further approaches like use of sacrificial layers or crystalline reinforcements in barrier coatings have attempted to mitigate CMAS propagation onto the surface of barrier coatings which only provided limited achievement. However, due to thermal mismatch between Al_2O_3 barrier layers, continuous detrimental effect was observed during thermal cycles [16,17].

Various T/EBCs materials and CMCs have been studied for CMAS attack to understand the recession behaviour of coatings and substrates [18–20]. For instance, SiC CMCs have been researched for its corrosion and mechanical behaviour extensively [21,22].On the other hand, counterparts of SiC/SiC composites i.e., oxide CMCs are examined very limitedly under similar conditions [23,24]. Hence, our previous paper

* Corresponding author. Department of Aerospace and Aircraft Engineering, Kingston University, Roehampton Vale Campus, London, SW15 3DW, United Kingdom.
** Corresponding author.
E-mail addresses: k1825123@kingston.ac.uk (K. Ramachandran), d.daniel@kingston.ac.uk (D.D. Jayaseelan).

https://doi.org/10.1016/j.ceramint.2023.10.214
Received 14 August 2023; Received in revised form 16 October 2023; Accepted 19 October 2023
Available online 23 October 2023

focused on understanding the effect of CMAS corrosion on O-O CMCs (AS-N610) at low temperature (800 °C to 1000 °C) with respect to time [25]. This study is a continuation to close the gap to understand the CMAS corrosion behaviour on oxide CMCs (AS-N610) at high temperature at 1200 °C and 1400 °C for different time intervals (1, 5 and 10 h).

2. Experimental details

2.1. Materials

Commercially available O-O CMCs (AS-N610) were provided by Ansaldo Energia, Italy which was prepared by COI ceramics, CA by infiltration of sol-gel derived aluminosilicate precursors followed by vacuum bagging and pressureless sintering. The samples of dimension of 10 × 10 × 3 mm for the corrosion studies were prepared through waterjet cutting (Custom waterjet cutting Ltd., Uxbridge, UK). The properties of O-O CMCs are reported in Table 1 [23]. For CMAS coating, powders of calcium oxide (CaO), magnesium oxide (MgO), silicon oxide (SiO_2) and aluminium oxide (Al_2O_3) with an average purity of ~98% and particle size of ~70 μm were obtained from Fishers Scientific Pvt. Ltd, United Kingdom.

2.2. CMAS preparation

CMAS composition towards this study was chosen based on previous studies [12,13,25]. The CMAS mixture consisted of 52.3 wt% SiO_2, 37.1 wt% CaO, 7.1 wt% Al_2O_3 and 3.5 wt% MgO was mixed with ethanol in a 1:2 ratio and wet ball milled (Planetary ball milling, Retsch, Germany) at a speed of 300 rpm for 4 h with 5 min intermediate resting time every half hour. The prepared slurry was heat treated at 1200 °C for 4 h and resultant powder was crushed using mortar/pestle and #500 mesh sieve was used for screening the powder.

2.3. CMAS coating

The synthesised CMAS powder was mixed with distilled water at a 2:1 ratio to form thick slurry. The O-O CMCs were dipped onto thick slurry for 60 s on one side and retracted slowly and dried at room temperature for 24 h and further dried at 200 °C for 2 h with slow heating and cooling rate of 1 °C/min.

2.4. Characterisation & testing methods

The oven dried CMAS coated oxide CMCs were further heat treated in a box furnace (Carbolite Gero, United Kingdom) to investigate the effect of CMAS corrosion on oxide CMCs at two different temperatures, 1200 °C and 1400 °C in various time intervals of 1, 5 and 10 h. For corrosion studies, CMAS coated O-O CMC samples were placed on a wedged alumina crucible to minimise contact between crucible and substrate. The samples were heated to desired temperature with a heating and cooling rate of 2 °C/min and held for different lengths of time at desired temperature.

The characterisation techniques such as X-ray diffraction (XRD) (Bruker D8) and scanning electron microscopy (SEM) (Zeiss SM350D) fitted with energy dispersive spectrometer (EDS) (Oxford Instruments) were used to analyse distinct phases and surfaces of heat-treated samples. For SEM and EDS analysis, samples were coated with Au/Pt through sputter coatings and XRD was carried out with values of 2θ ranging from 0 to 90° with step rate of 0.01° s^{-1}.

3. Results & discussion

The characterisation of O-O CMCs and synthesised CMAS are reported in our previous work [25]. The O-O CMCs had a typical fibre orientation of 0°/90° with Nextel™610 continuous woven fibres in aluminosilicate matrix with elemental distribution of silicon, aluminium and oxygen. Likewise, synthesised CMAS contained traces of anorthite ($CaAl_2Si_2O_8$), corundum (α-Al_2O_3) and diopside ($CaMgSi_2O_7$) which proved the presence of CMAS as it was in good agreement with previous studies [25,26].

3.1. Effect of CMAS on O-O CMCs

The dip-coated O-O CMCs were heat treated at 1200 °C and 1400 °C at different time intervals (1, 5 &10 h) in box furnace to understand the effect of CMAS corrosion. The weight change of the coated oxide CMCs was measure prior and after corrosion. The results show a clear weight gain due to good to adherence between O-O CMCs and CMAS coating which was result of longer rest time i.e., 24 h drying period prior to heat treatment. Table 2 shows the weight gain with respect to temperature, and it could be observed that O-O CMCs in presence of CMAS for 1 h indicated only negligible weight gain at 1200 °C and 1400 °C. On the contrary, samples corroded at 5 and 10 h indicated a linear weight gain at a scale of ~3% which could have been due to the formation of glassy phases of the CMAS onto the O-O CMCs. At elevated temperatures, CMAS diffuses into different oxides on the surface due to the lower transitional temperature (~800 °C) of CMAS which decreases the wetting and viscosity of CMAS leading it to penetrate porous oxide CMCs [27]. The weight gain on the corroded samples were minimum inferring that oxide layers formed from CMAS limited owing to pre-occurring oxide structure of CMCs and CMAS. The weight gain on CMAS coated O-O CMCs could also be associated with phase changes in CMAS with respect to the temperature. Our previous study revealed that the CMAS underwent new phase formation with increase in temperature into α-Al_2O_3 as well as diopside ($CaMgSi_2O_7$) and anorthite ($CaAl_2Si_2O_8$) up to 1000 °C which could have enhanced the weight gain onto the O-O substrate [25]. Further, with increase in temperature formation of Al_2SiO_5 could be imminent due to the decomposition of anorthite between 1100 °C and 1400 °C as per Eq. (1). With further increase in the temperature, Al_2SiO_5 may decompose back to form Al_2O_3 and SiO_2 as per Eq. (2) [28,29].

$$3CaAl_2Si_2O_8 \rightarrow Ca_3Al_2Si_3O_{12} + 2Al_2SiO_5 + SiO_2 \quad (1)$$

$$Al_2SiO_5 \rightarrow Al_2O_3 + SiO_2 \quad (2)$$

The cross-sectional surfaces of corroded samples were characterized

Table 2
Weight gain on CMAS coated O-O samples after corrosion test at different time intervals.

Duration / Temperature	1 h	5 h	10 h
1200°C	0.121 g	0.1224 g	0.128 g
1400°C	0.121 g	0.126 g	0.132 g

Table 1
Material description of AS-N610 oxide CMCs.

Material	Density (g/cm^3)	Nominal Fibre Volume (%)	Nominal Matrix volume (%)	Open Porosity (%)	Thermal expansion (10^{-6}/°C)	Maximum expansion temperature (°C)
AS-N610	2.83	51	49	25	8.0	1000

through X-ray diffraction (XRD) to understand the effect of CMAS onto the O-O CMCs. Most peaks of the samples heat treated for 1 h with CMAS at 1200 °C and 1400 °C is illustrated in Fig. 1 which corresponded to α-Al_2O_3 (corundum) along with presence of mullite, anorthite and Al_2SiO_5. The presence of mullite and alumina supports the composition of substrate which was fabricated with help of Nextel fibers made up of alumina and mullite matrix. Further, traces of the anorthite and presence of Al_2SiO_5 in the XRD supports penetration of the CMAS into the oxide CMCs. With increase in the corrosion time, most peaks diminished and further anorthite peaks considerably reduced. This could be due to the decomposition of the anorthite as per Eq. (1) and Eq. (2). The cross sectional XRD patterns at elevated temperature is represented in Fig. 2 which show the diminished peaks of the anorthite and Al_2SiO_5 which could have been due to formation of alumina or release of SiO_2. Due to lower Gibbs activation energy of alumina compared to SiO_2, formation of alumina would have been faster [30]. Most of the peaks correspond to α-Al_2O_3 and mullite ($3Al_2O_3$:$2SiO_2$) at both temperatures. With further increase in the temperature and corrosion time, the peaks of anorthite completely diminished by the decomposition of the anorthite. Also, there was a peak shift in the XRD at various peaks which might have been due to the utilisation of dip coatings which may attribute towards change in lattice constants [31].

The microstructural observation of the CMAS coated O-O CMCs is illustrated in Fig. 3. From Fig. 3, it could be observed that CMAS attained its transitional glassy temperature state at ~800 °C which led to melting of CMAS onto the porous structures as well as phase changes at 1200 °C and 1400 °C at 10 h with small amount of CMAS layer deposition on the surfaces of the O-O CMCs. This could have been due to the adherence between the substrates and CMAS during the heat treatment. On the other hand, in Fig. 4(b) cracks were observed on the intermediate region between CMCs and CMAS surfaces which could have been due to the thermal mismatch between the two different materials which led to continuous crack propagation throughout the surface of CMAS [32]. The EDS on the spots A and B marked in Fig (4) supported the evidence of CMAS on the surfaces with elemental compositions corresponding towards calcium (26.43 wt%), aluminium (16.24 wt%), silicon (8.16 wt%) and oxygen (39.24 wt%).

Further, microstructural evaluation on the CMAS coatings indicated delamination layers at 1200 °C/5 h propagating inwards towards the matrices as illustrated in Fig. 4(a). This crack propagation on the surface of coatings could be due to release of the in-plane stain energy [33]. Further, crack propagation could also be caused due to thermal mismatch between the CMAS (~10.25 × 10^{-6} K^{-1}) and O-O CMC (8 × 10^{-6} K^{-1}) substrate as illustrated in Fig. 4(b). Fig. 4(c) represents the

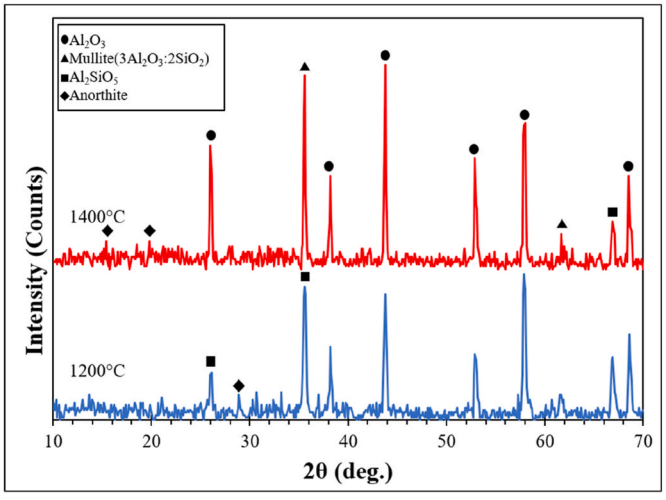

Fig. 1. Cross sectional X-ray diffraction pattern of heat treated CMAS coated O-O CMCs at 1200 °C and 1400 °C for 1 h.

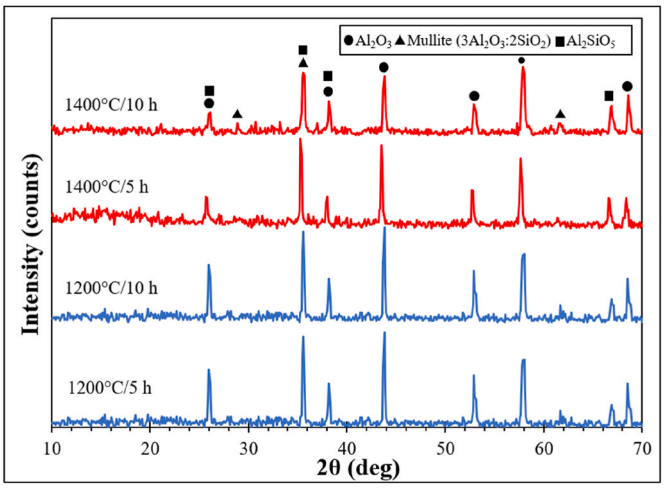

Fig. 2. X-ray diffraction patterns of CMAS coated O-O CMCs after heat treatment at 1200 °C and 1400 °C for 5 h and 10 h.

crack propagation from CMAS onto the matrices and fibres of substrate at 1400 °C/10 h. This could have been the reason at high temperature when the CMAS melts which may lead to wicks in the matrices of the columns of the porous CMCs leading to failure. The crack on the surfaces of matrices propagates to fibers of the O-O CMCs which may be due to stress transfer mechanism between the matrix and reinforcements [34]. The elemental distribution of the CMAS corroded oxide CMCs are reported in Table 3 which showcases presence of CMAS on the surface of oxide CMC substrate in both spots A and spot B. With increase in the holding duration, CMAS melted and penetrated the O-O substrate with presence of calcium aluminosilicate (CAS) with small quantity of Mg on the surfaces. The presence of CAS supports the damage/degradation which may take place on the O-O CMCs. However, black pigmentation of the CAS with small Mg quantity was not noticed on the surfaces of the O-O CMCs as reported in previous research works [21,25].

3.2. *Effect of CMAS on fracture toughness*

Fracture toughness of the CMAS coated O-O CMCs after heat treatment was calculated through indentation technique to understand the effect on CMAS onto the substrate. The indentation fracture toughness of O-O at ambient condition was 7.78 ± 0.5 MPa $m^{0.5}$ which was closer to previous reports [22,25,35]. However, after heat treatment in presence of CMAS at elevated temperatures, fracture toughness of the O-O CMCs reduced as reported in Table 4. From Tables 3 and it can be inferred that the samples heat treated with CMAS at 1200 °C and 1400 °C for 10 h highlighted a reduction of ~14% and ~22% compared to room temperature sample. However, fracture toughness deterioration at 1200 °C was ~3% higher to samples at 1000 °C which was reported in our previous work [25].

The deterioration of the fracture toughness is attributed to the infiltration of CMAS onto the porous substrate which could have wicked the matrices and fibres of O-O CMCs. Further, the corrosion occurring due to the CMAS infiltration could have weaken the toughness. Degradation on the mechanical properties due to brittle fracture of oxide CMCs (with Nextel^{TM}720 fibers) have been previously reported [22]. The SE images (Fig. 4(a) and (b)) indicated no visible fractures at 1200 °C at both the time duration, however samples heat-treated at 1400 °C/10 h indicated fractures on the fibres closer to area where CMAS melted region as illustrated in Fig. 5. The EDS analysis of the melted CMAS region near the fibres indicated a mixture of CAS (calcium aluminosilicate) with elemental composition of calcium (6.28 wt%), aluminium (34.16 wt%), silicon (20.45 wt%) and oxygen (34.29 wt%) along with small traces of magnesium (0.18 wt%). However, there was

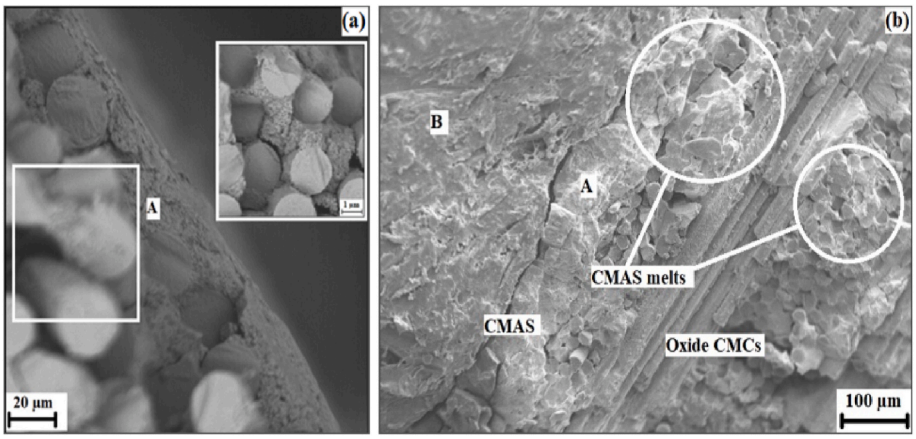

Fig. 3. Cross-sectional microstructural view on coating at (a) 1200 °C/10 h and (b) 1400 °C/10 h.

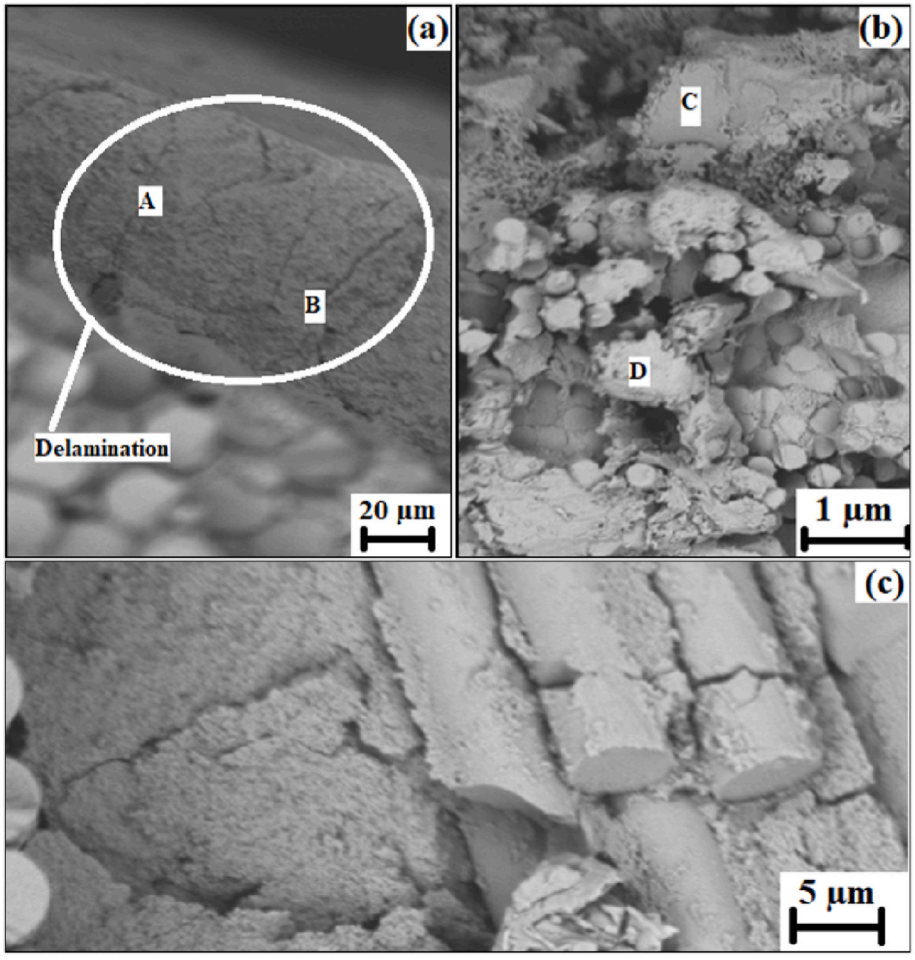

Fig. 4. (a) Delamination on CMAS coatings propagating inwards towards the substate at 1200 °C/5 h, (b) Crack formation due to the thermal mismatch between CMAS and O-O CMCs 1200 °C/10 h and (c) Crack propagation onto the oxide fibers from the matrices 1400 °C/10 h.

no degradation on the matrices and fibres. The drop in the fracture toughness of the O-O CMCs could have been also due to phase transition/formation of the alumina which have lower fracture toughness while undergoing the corrosion [36].

4. Conclusion

High temperature corrosion behaviour and the fracture toughness of O-O CMCs coated with CMAS through dip coatings were studied using different characterisation techniques for its utilisation in high temperature turbine and its components. The corrosion behaviour showed negligible weight gain at 1200 °C and 1400 °C for 1 h time duration. However, with increase in corrosion time the weight also enhanced leading to maximum increase of ~3% for samples heat-treated for 1400 °C/10 h. The XRD technique reveals that after CMAS corrosion, alumina and mullite were present as dominant phases along with small

Table 3
Elemental distribution of CMAS corroded O-O CMCs in Fig. 4

Elements Region	Al (wt.%)	Si (wt.%)	O (wt.%)	Ca (wt.%)	Mg (wt.%)
Spot A	12.38	10.71	47.42	18.22	4.26
Spot B	28.08	18.86	34.19	10.43	2.20
Spot C	26.76	15.08	29.06	16.18	2.92
Spot D	21.34	12.46	40.85	21.59	0.49

Table 4
Fracture toughness of CMAS corroded O-O CMCs after 10 h.

Temperature	Fracture Toughness ($MPa.m^{0.5}$)
Room Temperature	7.78 ± 0.5
1200 °C	6.65 ± 0.4
1400 °C	6.02 ± 0.5

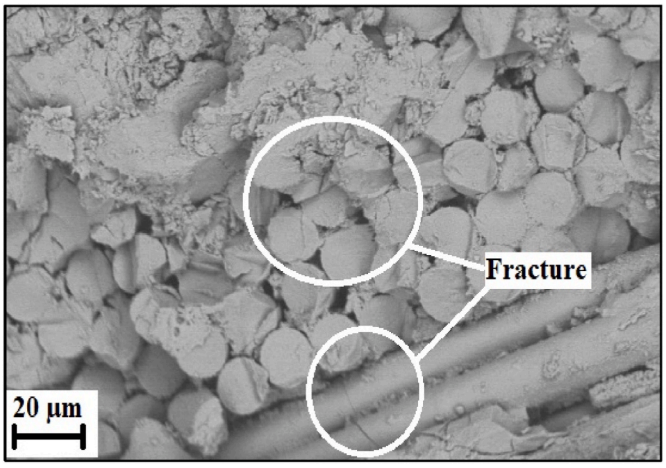

Fig. 5. Fracture on the surfaces of oxide fibers after 1400 °C/10 h.

traces of CMAS constituents which indicates the thermal stability of oxide CMCs at high temperature of 1400 °C. With increase in corrosion time, there were delamination on the surfaces of CMAS which propagated onto the substrate leading to cracks on the matrices and fibres. The EDS spotting picked up traces of calcium aluminosilicate (CAS) with small Mg percentage which could have wicked the columns of the substrate leading to cracks. The indentation fracture toughness of the O-O CMCs after corrosion indicated a drop of ~22% for samples corroded at 1400 °C for 10 h.

Data availability

Data towards this research will be made available upon request.

Declaration of competing interest

The authors declare that they have no known competing financial interests or personal relationships that could have appeared to influence the work reported in this paper.

Acknowledgement

Authors Karthikeyan Ramachandran would like to acknowledge Kingston University, United Kingdom for support towards his PhD research. Authors would also acknowledge the thank Senior Technicians in Kingston University, Mr. Dean Wells and Mr. Simon Crust for their support in experimental and characterisation procedures.

References

[1] L. Sun, Y. Luo, Z. Tian, X. Ren, J. Li, W. Hu, J. Zhang, J. Wang, High temperature corrosion of (Er0.25Tm0.25Yb0.25Lu0.25)2Si2O7 environmental barrier coating material subjected to water vapor and molten calcium–magnesium–aluminosilicate (CMAS), Corrosion Sci. 175 (2020), 108881.
[2] J.C. Williams, E.A.S. Jr, Progress in structural materials for aerospace systems, Acta Mater. 51 (19) (2003) 5775–5799.
[3] H. ohnabe, S. Masaki, M. Onozuka, K. Miyahara, T. Sasa, Potential application of ceramic matrix composites to aero-engine components, Compos. Appl. Sci. Manuf. 30 (4) (1999) 489–496.
[4] N.A. Nasiri, N. Patra, N. Ni, D.D. Jayaseelan, W.E. Lee, Oxidation behaviour of SiC/SiC ceramic matrix composites in air, J. Eur. Ceram. Soc. 36 (14) (2016) 3293–3302.
[5] N.A. Nasiri, N. Patra, D.D. Jayaseelan, W. Lee, Water vapour corrosion of rare earth monosilicates for environmental barrier coating application, Ceram. Int. 43 (10) (2017) 7393–7400.
[6] A. Aygun, A.L. Vasiliev, N.P. Padture, X. Ma, Novel thermal barrier coatings that are resistant to high-temperature attack by glassy deposits, Acta Mater. 55 (20) (2007) 6734–6745.
[7] D.D. Jayaseelan, Y. Xin, L. Vandeperre, P. Brown, W. Lee, Development of multi-layered thermal protection system (TPS) for aerospace applications, Compos. B Eng. 79 (2015) 392–405.
[8] C.G. Levi, J.W. Hutchinson, M.H. Vidal-Setif, C.A. Johnson, Environmental degradation of thermal-barrier coatings by molten deposits, MRS Bull. 37 (2012) 932–941.
[9] V. Wiesner, B. Harder, N. Bansal, High-temperature interactions of desert sand CMAS glass with yttrium disilicate environmental barrier coating material, Ceram. Int. 44 (18) (2018) 22738–22743.
[10] R. Wellman, G. Whitman, J. Nicholls, CMAS corrosion of EB PVD TBCs: identifying the minimum level to initiate damage, Int. J. Refract. Metals Hard Mater. 28 (1) (2010) 124–132.
[11] J.G. Thakare, C. Pandey, M. Mahapatrea, R. Mulik, Thermal barrier coatings—a state of the art review, Met. Mater. Int. 27 (2021) 1947–1968.
[12] J.M. Drexler, A.L. Ortiz, N.P. Padture, Composition effects of thermal barrier coating ceramics on their interaction with molten Ca–Mg–Al–silicate (CMAS) glass, Acta Mater. 60 (15) (2012) 5437–5447.
[13] S. Kramer, J. Yang, C.G. Levi, Thermochemcial interaction of thermal barrier coatings with molten CaO-MgO-Al2O3-SiO2 (CMAS) deposits, J. Am. Ceram. Soc. 89 (10) (2006) 3167–3175.
[14] H.-F. Chen, C. Zhang, Y.-C. Liu, P. Song, W.-X. Li, G. Yang, B. Liu, Recent progress in thermal/environmental barrier coatings and their corrosion resistance, Rare Met. 39 (2020) 498–512.
[15] B. Li, Z. Chen, H. Zheng, G. Li, H. Li, P. Peng, Wetting mechanism of CMAS melt on YSZ surface at high temperature: first-principles calculation, Appl. Surf. Sci. 483 (2019) 811–818.
[16] V. Kumar, K. Balasubramanian, Progress update on failure mechanisms of advanced thermal barrier coatings: a review, Prog. Org. Coating 90 (2016) 54–82.
[17] R. Darolia, B. Nagaraj, Method of forming a coating resistant to deposits and coating formed thereby, US Patent 6 (2002) 720, 038.
[18] J.J.G. Chavez, R. Naraparaju, P. Mechnich, K. Kelm, U. Schulz, C. Ramana, Effects of yttria content on the CMAS infiltration resistance of yttria stabilized thermal barrier coatings system, J. Mater. Sci. Technol. 43 (2020) 74–83.
[19] N.L. Ahlborg, D. Zhu, Calcium–magnesium aluminosilicate (CMAS) reactions and degradation mechanisms of advanced environmental barrier coatings, Surf. Coating. Technol. 237 (2013) 79–87.
[20] G. Cao, Y.-H. Wang, Z.-Y. Ding, Z.-G. Liu, J.-H. Ouyang, Y.-M. Wang, Y.-J. Wang, CMAS hot corrosion behavior of rare-earth silicates for environmental barrier coatings applications: a comprehensive review, Heat Treatment and Surface Engineering 3 (1) (2021) 9–28.
[21] D.C. Faucett, S.R. Choi, Strength degradation of Oxide/Oxide and SiC/SiC ceramic matrix composites in CMAS and CMAS/Salt exposures, in: ASME 2011 Turbo Expo: Turbine Technical Conference and Exposition, Vancouver, British Columbia, Canada, 2011.
[22] S.R. Choi, C. Faucett, Combined effects of CMAS and FOD in ceramic matrix composites, in: ASME Turbo Expo 2012: Turbine Technical Conference and Exposition, Copenhagen, Denmark, 2012.
[23] K. Ramachandran, S. Leelavinodhan, C. Antao, A. Copti, C. Mauricio, Y. Jyothi, D. D. Jayaseelan, Analysis of failure mechanisms of Oxide - oxide ceramic matrix composites, J. Eur. Ceram. Soc. 42 (4) (2022) 1626–1634.
[24] V. Kostopoulos, T.H. Loutas, A. Kontsos, G. Sotiriadis, Y.Z. Pappas, On the identification of the failure mechanisms in oxide/oxide composites using acoustic emission, NDT E Int. 36 (8) (2003) 571–580.
[25] K. Ramachandran, B. Chaffey, C. Zuccarini, J.C. Bear, D. Jayseelan, Experimental and mathematical modelling of corrosion behaviour of CMAS coated oxide/oxide CMCs, Ceram. Int. 49 (3) (2022) 4213–4221.
[26] C. Mikulla, R. Naraparaju, U. Schulz, F.-L. Toma, M. Barbosa, L. Steinberg, C. Leyens, Investigation of CMAS resistance of sacrificial suspension sprayed alumina topcoats on EB-PVD 7YSZ layers, J. Therm. Spray Technol. 29 (2020) 90–104.
[27] B. Yin, M. Sun, W. Zhu, L. Yang, Y. Zhou, Wetting and spreading behaviour of molten CMAS towards thermal barrier coatings and its influencing factors, Results Phys. 26 (104365) (2021) 1–10.
[28] J.R. Goldsmith, The melting and breakdown reactions of anorthite at high pressures and temperatures, Am. Mineral. 65 (1980) 272–284.

[29] A. Friedrich, M. Kunz, B. Winkler, T.l. Bihan, High-pressure behavior of sillimanite and kyanite: compressibility, decomposition and indications of a new high-pressure phase, Z. für Kristallogr. - Cryst. Mater. 219 (6) (2009).
[30] K. Ramachandran, Z. Carmine, K. Ypshida, T. Tsunoura, D.D. Jayaseelan, Experimental investigation and mathematical modelling of water vapour corrosion of Ti3SiC2 and Ti2AlC ceramics and their mechanical behaviour, J. Eur. Ceram. Soc. 41 (9) (2021) 4761–4773.
[31] G. Vourlias, Application of X-rays diffraction for identifying thin oxide surface layers on zinc coatings, Coatings 10 (1005) (2020) 1–14.
[32] T.-Z. Tu, J.-X. Liu, L. Zhou, Y. Liang, G.-J. Zhang, Graceful behavior during CMAS corrosion of a high-entropy rare-earth zirconate for thermal barrier coating material, Journal of the European Ceramic Scoeity 42 (2) (2022) 649–659.
[33] C. Mercer, S. Faulhaber, A. Evans, R. Darolia, A delamination mechanism for thermal barrier coatings subject to calcium–magnesium–alumino-silicate (CMAS) infiltration, Acta Mater. 53 (4) (2005) 1029–1039.
[34] K.H. Khafagy, C. Sorini, T. Skinner, A. Chattopadhyay, Modeling creep behavior in ceramic matrix composites, Ceram. Int. 47 (9) (2021) 12651–12660.
[35] M. Ruggles-Wrenn, T. Kutsal, Effects of steam environment on creep behavior of Nextel™720/alumina–mullite ceramic composite at elevated temperature, Compos. Appl. Sci. Manuf. 41 (12) (2010) 1807–1816.
[36] K. Ramachandran, R.R. Subramani, T. Arunkumar, V. Boopalan, Mechanical and thermal properties of spark plasma sintered Alumina-MWCNTs nanocomposites prepared via improvised colloidal route, Mater. Chem. Phys. 272 (125034) (2021) 1–9.